

## [15] Voxelation Methods for Genome Scale Imaging of Brain Gene Expression

By DANIEL M. SFORZA and DESMOND J. SMITH

### Introduction

Imaging techniques have granted access to significant results on structure and function in the central nervous system. In addition, the completion of the human genome sequence promises to accelerate even further the already extraordinary developments of molecular biology. Therefore it is a natural step to seek an integration of both fields for a better understanding of the molecular basis of the brain. One strategy employs reporter genes, and this has been a major advance in molecular imaging. However, although this approach has important advantages, such as *in vivo* imaging, it does not provide convenient access to genome-wide information but only the examination of one, or at most, a few genes at a time.<sup>1-5</sup> One recently developed approach for genome-scale acquisition of brain gene expression patterns employs microarray analysis of spatially registered voxels (cubes) harvested from the brain.<sup>6,7</sup> This method is called voxelation and provides a mapping of gene expression analogous to the images reconstructed in biomedical imaging techniques, such as X-ray computerized tomography (CT), positron emission tomography (PET), and magnetic resonance imaging (MRI).

Voxelation has permitted high-throughput gene expression reconstructions in human and rodent brains.<sup>8-11</sup> One study using human brains compared gene expression between brains from normal individuals and brains

<sup>1</sup> S. S. Gambhir, J. R. Barrio, H. R. Herschman, and M. E. Phelps, *Nucl. Med. Biol.* **26**, 481 (1999).

<sup>2</sup> S. S. Gambhir, J. R. Barrio, H. R. Herschman, and M. E. Phelps, *J. Nucl. Cardiol.* **6**, 219 (1999).

<sup>3</sup> H. R. Herschman, D. C. MacLaren, M. Iyer, M. Namavari, K. Bobinski, L. A. Green, L. Wu, A. J. Berk, T. Toyokuni, J. R. Barrio, S. R. Cherry, M. E. Phelps, E. P. Sandgren, and S. S. Gambhir, *J. Neurosci. Res.* **59**, 699 (2000).

<sup>4</sup> A. Y. Louie, M. M. Huber, E. T. Ahrens, U. Rothbacher, R. Moats, R. E. Jacobs, S. E. Fraser, and T. J. Meade, *Nat. Biotechnol.* **18**, 321 (2000).

<sup>5</sup> D. A. Zacharias, G. S. Baird, and R. Y. Tsien, *Curr. Opin. Neurobiol.* **10**, 416 (2000).

<sup>6</sup> D. Liu and D. J. Smith, *Methods* **31**, 317 (2003).

<sup>7</sup> R. P. Singh and D. J. Smith, *Biol. Psychiatry* **53**, 1069 (2003).

<sup>8</sup> V. M. Brown, A. Ossadtchi, A. H. Khan, S. R. Cherry, R. M. Leahy, and D. J. Smith, *Genome Res.* **12**, 244 (2002).

<sup>9</sup> V. M. Brown, A. Ossadtchi, A. H. Khan, S. Yee, G. Lacan, W. P. Melega, S. R. Cherry, R. M. Leahy, and D. J. Smith, *Genome Res.* **12**, 868 (2002).

from individuals with Alzheimer's disease.<sup>8</sup> The mouse studies investigated global gene expression patterns in brains of a Parkinson's disease model induced by toxic doses of methamphetamine compared with controls.<sup>9</sup>

The previously mentioned voxelation studies used fresh tissue slabs, but a weakness of this approach is the deformation of the tissue during the process of physical voxelation, which can make problematic the registration of gene expression analysis results to the neuroanatomy. Although this is not a major problem for low-resolution studies, it becomes a significant factor at higher resolution. Therefore we have developed a new voxelation protocol to overcome this drawback and make feasible higher-resolution studies.<sup>12</sup> The new procedure involves the use of a fixation process to avoid tissue deformation and to allow histologic staining,<sup>13</sup> as well as cryoprotection to allow harvesting of slabs from frozen specimens.<sup>14</sup> These protocols have been shown to preserve RNA quality and yield at excellent levels, and allow the use of quality demanding downstream applications such as real-time polymerase chain reaction (PCR) or DNA microarrays.<sup>12</sup>

In the following sections we review the complete protocols and methods for high-resolution voxelation, from samples preparation to data analysis and image reconstruction.

## Methods

The following protocol can be applied to rodent or monkey studies and requires the use of intercardiac perfusion. Here we provide the times and volumes of the solutions used for adult C57BL/6J male mice (10 to 24 weeks, 25 to 31 g) for which the protocol was developed,<sup>12</sup> but it can be easily adapted to the other cases. For all perfusions, a small mechanical pump was used that allowed a flux of  $1.5 \text{ ml min}^{-1}$ . To easily switch among the different solutions and avoid the formation of bubbles, a serial connection of three-way stopcocks with swivel male luer lock was used (MX231-1L; Medex, Hilliard, OH) and carefully filled with the solutions before starting the procedure.

---

<sup>10</sup> A. Ossadtchi, V. M. Brown, A. H. Khan, S. R. Cherry, T. E. Nichols, R. M. Leahy, and D. J. Smith, *Neurochem. Res.* **27**, 1113 (2002).

<sup>11</sup> R. P. Singh, V. M. Brown, A. Chaudhari, A. H. Khan, A. Ossadtchi, D. M. Sforza, A. K. Meadors, S. R. Cherry, R. M. Leahy, and D. J. Smith, *J. Neurosci. Methods* **125**, 93 (2003).

<sup>12</sup> D. M. Sforza, J. Annese, D. Liu, S. Levy, A. W. Toga, and D. J. Smith, *Neurochem. Res.* **29**, 1291 (2004).

<sup>13</sup> J. Annese and A. W. Toga, in "Brain Mapping: The Methods" (A. W. Toga and J. C. Mazziotta, eds.), p. 537. Academic Press, New York, 2002.

<sup>14</sup> D. L. Rosene and K. J. Rhodes, in "Methods in Neuroscience, Vol. 3: Quantitative and Qualitative Microscopy" (P. M. Conn, ed.), p. 360. Academic Press, New York, 1990.

### *Sample Preparation*

1. Mice must undergo intracardiac perfusion under deep halothane anesthesia. For each animal the vasculature is cleared with 11–22 ml of ice-cold phosphate buffered saline solution (PBS).
2. Fixation: 67 ml of 4% paraformaldehyde in PBS (pH 7.4) is perfused for a period of 45 min.
3. Cryoprotection: mice are additionally perfused with 67 ml of 10%, 20%, and 30% ice-cold phosphate buffered sucrose solutions (pH 7.4). The sucrose solutions are each perfused for 45 min.
4. After perfusion, brains are removed from the skull and immediately frozen in chilled isopentane or liquid nitrogen. Tissue blocks are kept at  $-70^{\circ}$  until RNA testing and histologic processing.

This complete protocol lasts approximately 190 minutes.

### *Histologic Staining*

As voxelation studies are pushed to higher resolution, registration between the harvested voxels and the neuroanatomy becomes increasingly important. At lower levels of resolution, visual inspection and digital photographs of fresh sections are sufficient for registration. However, the inherent low contrast of fresh specimens makes it difficult to identify boundaries between structures of small size or subtly different microscopic anatomy, and this hinders image reconstruction at high resolution. Proper use of the described fixation and cryoprotection protocol allows the use of histologic stains to improve contrast in the voxelated section and facilitate image registration. There are methods available for histologic staining of tissue compatible with the recovery of good quality RNA for gene expression studies.<sup>15</sup>

### *Physical Voxelation*

The equipment required for voxelation depends on the specimen under study and on the desired resolution. A detailed description of voxelation devices and procedures for human and rodent species can be found in Liu and Smith.<sup>6</sup> Furthermore, supplementary information on the design and construction of these pieces of equipment (including blueprints) is given at our web site (<http://pharmacology.ucla.edu/smithlab/>). The devices essentially consist of two-dimensional arrays of blades, together with

<sup>15</sup> P. Bonaventure, H. Guo, B. Tian, X. Liu, A. Bittner, B. Roland, R. Salunga, X. J. Ma, F. Kamme, B. Meurers, M. Bakker, M. Jurzak, J. E. Leysen, and M. G. Erlander, *Brain Res.* **943**, 38 (2002).

supporting and guiding mechanisms to facilitate registered harvesting of voxels. Voxelation devices have been constructed that harvest square voxels of size 3.3 mm (used in the human studies, a 425-voxel template, consisting of 25 voxels in length and 17 voxels in width) to 1 mm (used in the rodent studies, a 400-voxel template,  $20 \times 20$  voxels).<sup>11</sup>

The selection of the actual section for voxelation obviously depends on the nature of the investigation. At the moment all voxelation studies have investigated coronal sections. Human studies on Alzheimer's disease focused on left coronal hemisections that included the hippocampus, corresponding to section 17 of the University of Maryland Brain and Tissue Bank protocol, method 2 (<http://medschool.umaryland.edu/BTBank/>).<sup>8</sup> The thickness of the slab is also an important factor in order to obtain enough RNA for microarray hybridization, as well as for the accuracy of the regions identified on the section. In the human studies, the slice thickness was 8 mm. In the study of the mouse model of Parkinson's disease,<sup>9</sup> a different strategy was applied. The whole brain was divided into slices of thickness 1 mm using a brain matrix (Harvard Apparatus, Inc., Holliston, MA). Each slice was then divided into four voxels, giving a total of 40 voxels, and an average volumetric resolution of  $7.5 \mu\text{l}$ . The existence of voxelation instruments for the rodent brain will allow acquisition of expression images at 1 mm ( $1 \mu\text{l}$ ) resolution.<sup>11</sup>

It is important to obtain digital pictures of the selected slab before and after voxelation in order to evaluate possible deformation induced by the procedure, as we already mentioned, this is more likely to be a problem as resolution is increased. In addition, digital pictures are required for image registration and reconstruction (see last section).

### *RNA Isolation and Quality Check*

There are many commercially available RNA isolation kits. Lately we have obtained excellent yields and quality using the RNeasy Lipid Tissue Mini Kit column (Qiagen, Hilden, Germany). Frozen samples are placed in QIAzol Lysis Reagent (Qiagen) and homogenized using a Tissue-Tearor homogenizer (BioSpec Products, Bartlesville, OK). Subsequent steps are done according to the instructions provided by the manufacturer of the RNeasy kit. Total RNA quality is assessed by microcapillary electrophoresis using the Agilent BioAnalyzer 2100 (Agilent Technologies, Palo Alto, CA). Evaluation of 18-s and 28-s RNA peaks and background noise are employed for this purpose.

The cryoprotection step is very important to achieve good RNA quality and recovery. It is well known that paraformaldehyde fixation results in an apparent decrease in both the recovery and quality of RNA extracted from

brain.<sup>16–18</sup> However, we have shown that sucrose perfusion following fixation helps preserve the RNA.<sup>12</sup>

The long time required for the complete protocol might raise doubts about RNA quality, but these are unfounded. Our experience is consistent with published work in the sense that the quality of RNA from human brains depends on brain pH, a measure of premortem condition, rather than postmortem interval.<sup>19</sup>

### *Microarrays, RNA Labeling, and Hybridization*

High-resolution voxelation requires the use of a large number of microarrays, so the use of spotted cDNA arrays is the natural option due to their relatively low cost. The list of clones used in published voxelation investigations can be obtained at our web site (<http://www.pharmacology.ucla.edu/smithlab/>). To produce targets for hybridization to the cDNA microarrays, 10  $\mu\text{g}$  of total RNA is labeled with fluorescent nucleotides by chemical coupling following reverse transcription. The total RNA is mixed with 6  $\mu\text{g}$  of anchored oligo-dT (5'-TTTTTTTTTTTTTTTTT VN-3') and hybridization achieved by incubation at 70° for 10 min, followed by 10 min at 4° in a total volume of 18  $\mu\text{l}$ . The annealed RNA is then reverse-transcribed in a 30- $\mu\text{l}$  reaction mix containing reaction buffer (50 mM Tris-HCl, 75 mM KCl, 3 mM MgCl<sub>2</sub>, pH 8.3); 10 mM dithiothreitol; 200  $\mu\text{M}$  dATP, dGTP, and dCTP; 51  $\mu\text{M}$  dTTP; 149  $\mu\text{M}$  amino-allyl-UTP (Sigma, St. Louis, MO); and 200U SuperScript II reverse transcriptase (Life Technologies, Gaithersburg, MD). The reactions are incubated at 42° for 2 h. Following incubation, 10  $\mu\text{l}$  of 1 M NaOH and 10  $\mu\text{l}$  of 0.5 M EDTA are added to degrade the template RNA, and the samples are incubated at 70° for 10 min. The reaction is neutralized by the addition of 10  $\mu\text{l}$  of 1 M HCl, followed by 300  $\mu\text{l}$  of Qiagen Buffer PB (PCR Cleanup kit; Qiagen, Valencia, CA). Reactions are purified using Qiagen's PCR cleanup kit following the manufacturer's directions with the substitution of 80% ethanol for Qiagen's PE buffer and water for Qiagen's EB buffer.

Following purification, individual samples are desiccated, resuspended in 7  $\mu\text{l}$  0.1 M sodium bicarbonate buffer, and chemically coupled to

<sup>16</sup> S. M. Goldsworthy, P. S. Stockton, C. S. Trempus, J. F. Foley, and R. R. Maronpot, *Mol. Carcinog.* **25**, 86 (1999).

<sup>17</sup> R. Parlato, A. Rosica, V. Cuccurullo, L. Mansi, P. Macchia, J. D. Owens, J. F. Mushinski, M. De Felice, R. F. Bonner, and R. Di Lauro, *Anal. Biochem.* **300**, 139 (2002).

<sup>18</sup> S. J. Scheidl, S. Nilsson, M. Kalen, M. Hellstrom, M. Takemoto, J. Hakansson, and P. Lindahl, *Am. J. Pathol.* **160**, 801 (2002).

<sup>19</sup> P. J. Harrison, P. R. Heath, S. L. Eastwood, P. W. Burnet, B. McDonald, and R. C. Pearson, *Neurosci. Lett.* **200**, 151 (1995).

monofunctional reactive cyanine dyes (Amersham Biosciences, Buckinghamshire, England). Unbound cyanine dyes are removed by purification with Qiagen's PCR cleanup kit as described earlier. Following purification, the labeled samples are combined in Cy3–Cy5 pairs, desiccated, and resuspended in 100  $\mu$ l hybridization buffer (25% formamide, 5  $\times$  SSC, 0.1% sodium dodecyl sulfate [SDS], 10  $\mu$ g yeast tRNA, 10  $\mu$ g poly-A-RNA, 1  $\mu$ g human COT-1 DNA). Immediately prior to hybridization, the microarrays are prehybridized in a solution of 5  $\times$  SSC, 1% SDS, and 1% bovine serum albumin (BSA) at 55° for 45 min. Following prehybridization, the arrays are vigorously washed in ddH<sub>2</sub>O to remove all traces of the prehybridization solution, rinsed in isopropanol, and dried at room temperature (RT).

The labeled RNA samples are denatured at 95° for 2 min and placed on the prehybridized arrays, covered with Lifterslip coverslips (25 mm  $\times$  60 mm; Erie Scientific, Inc., Portsmouth, NH), placed in a hybridization chamber (Corning, Acton, MA) with 30  $\mu$ l hybridization buffer to maintain humidity, and incubated at 42° for 16 h in a standard hybridization oven. After hybridization, the arrays are washed in 2  $\times$  SSC to remove the coverslips, placed in 2  $\times$  SSC, 0.1% SDS at 55° with agitation for 5 min then washed with two successive 5 min washes with 1  $\times$  SSC and 0.1  $\times$  SSC at RT. The washed arrays are dried by centrifugation at 50g for 5 min and immediately scanned using a GenePix 4000A microarray scanner (Axon Instruments, Union City, CA).

## Data Analysis

Voxelation studies yield large amounts of data, and a variety of different analytical techniques can be employed for data mining. There are low- and high-level analyses of the microarray data, described in the next two subsections. Also important is how to display the large amount of information retrieved from microarrays in a meaningful and appealing manner. This is discussed in the last subsection. Unless otherwise specified, all computational algorithms described are written in Matlab scripting language (Matlab 5.3 or later required) and can be retrieved from the lab web site (<http://www.pharmacology.ucla.edu/smithlab/>). The algorithms are run on a personal computer and are not highly demanding of resources, so a workstation is not required.

### *Low-Level Analysis*

Low-level analysis refers to image processing of scanned microarray images and normalization (within array and interarrays). Images are usually processed by the software bundle included with the scanner, and they

allow automatic spot segmentation and acquisition of intensity values in both channels. In our case the microarray scanner is a GenePix 4000A (Axon Instruments) with GenePix Pro 3.0 software. An important step is the normalization of the data to correct the multiple sources of systematic variation in cDNA microarray experiments that affect measured gene expression levels.<sup>20</sup> The normalization procedure we have applied in our studies consists of the removal of spatial trends due to array printing by a nonlinear transformation of the data set and the compensation for differences in the labeling of Cy3 and Cy5 dyes by aligning the histograms of the dye signals both within, as well as between, microarrays. The normalization method relies on the assumption that most of the genes do not change significantly between different experimental conditions.

### *High-Level Analysis*

After the data have been properly normalized, calculated gene expression values can be subjected to further analysis in the search of relevant biologic information. The most common first step in the analysis of the data is the identification of significantly changing expression values; this singles out genes that are upregulated or downregulated in the comparison between control and experimental conditions. Even more interesting is the identification of clusters of coregulated and antiregulated genes, which can potentially identify regulatory networks.<sup>8,9</sup>

There are also exploratory techniques that do not rely on a priori hypotheses or assumptions concerning the data, such as singular value decomposition. This method can identify clusters of genes (gene “vectors”) that most efficiently explain the variance in the data. It has been shown that these gene vectors display interesting regional patterns of expression, and their associated genes may play an important role in differentiation of the mouse and human brain.<sup>8,9</sup> In addition, a gene vector has been identified that shows a significant spatial shift away from the striatum in the normal mouse brain toward the hippocampus in the Parkinson’s brain.<sup>9</sup> These results suggest that high-throughput acquisition of gene expression patterns in combination with singular value decomposition has the potential to identify functionally abnormal neuroanatomic regions in neurologic disease states. This is especially relevant given the fact that for many neuropsychiatric disorders, such as schizophrenia, Down syndrome, and autism, the location of functionally abnormal brain regions associated with the diseases

<sup>20</sup> Y. H. Yang, S. Dudoit, P. Luu, D. M. Lin, V. Peng, J. Ngai, and T. P. Speed, *Nucleic Acids Res.* **30**, e15 (2002).

remains enigmatic. The higher-resolution gene expression images that can be obtained following the protocols described here would potentially allow the precise identification of such important regions, given that they exist.

Another technique that has proven powerful in modeling microarray data from voxelation is the analysis of variance (ANOVA).<sup>10,21,22</sup> With microarray data analysis, there is always an underlying question: how to calculate valid estimates of gene expression values that take into account potential sources of variation, both from experimental design and error. ANOVA can provide corrected estimates of change in gene expression with the estimation of potential confounding effects. The use of ANOVA to analyze voxelation data was found to produce results consistent with those from singular value decomposition.<sup>10</sup>

### *Image Reconstruction*

High-resolution voxelation can result in demanding data sets for image reconstruction. The addition of a staining step in the protocol can help greatly, especially at high resolution, as we have already discussed. The basic problem is to align an actual voxelated slab to a corresponding atlas image. The final image represents the overlapping of an anatomic image and gene expression levels converted into pseudocolor. The registration between the picture of the actual voxelated section and the atlas image is accomplished using an implementation of the thin-plate splines warping method.<sup>23</sup> This method interpolates surfaces between scattered fiducial landmarks, and its name refers to a physical analogy involving the bending of a thin sheet of metal subject to point constraints (the landmarks that relate both images). The manual selection of corresponding fiducial landmarks on both images allows the algorithm to warp the desired image onto the atlas reference. Gene expression images are further improved using interpolation and smoothing functions. For the high-resolution human expression images, the smoothing used about 2–4 voxels and for the high-resolution rodent images, only 1 voxel. Examples of final images obtained from voxelation are displayed in [Fig. 1](#).

<sup>21</sup> M. K. Kerr and G. A. Churchill, *Genet. Res.* **77**, 123 (2001).

<sup>22</sup> M. K. Kerr, M. Martin, and G. A. Churchill, *J. Comput. Biol.* **7**, 819 (2000).

<sup>23</sup> F. L. Bookstein, *IEEE Trans. Patt. Anal. Mach. Intell.* **11**, 567 (1989).

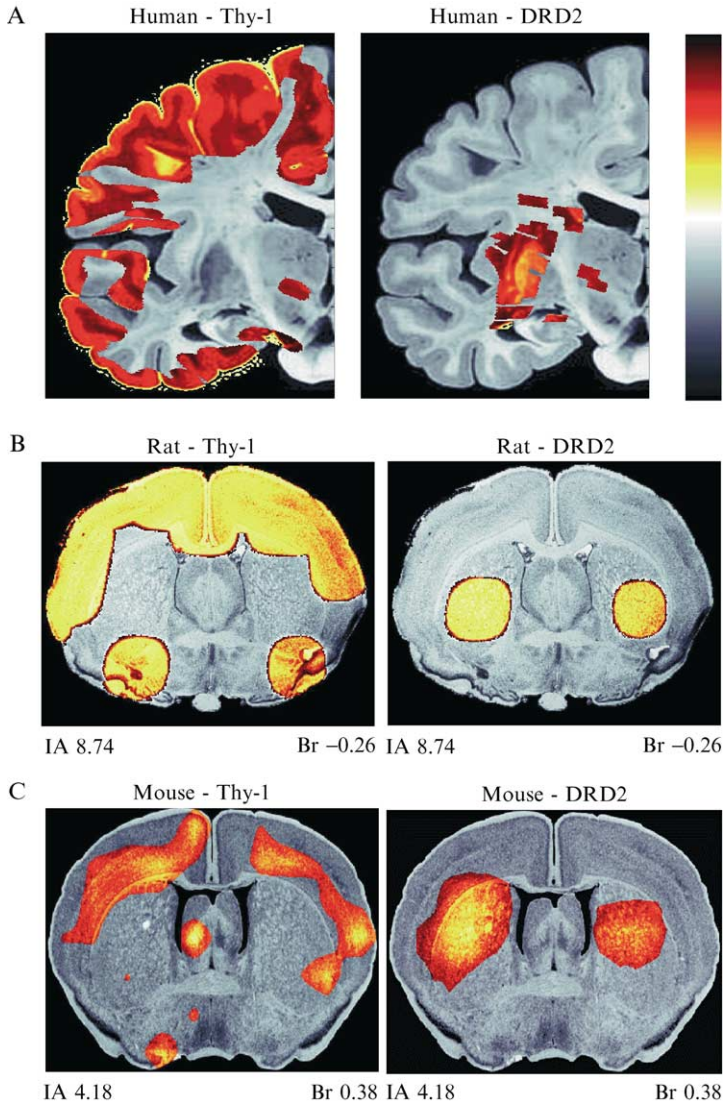


FIG. 1. Human and rodent brain voxelation gene expression images for Thy-1 and DRD2 (dopamine D2 receptor) genes. Images are the result of the methods explained in the text. Gene expression patterns are shown in pseudocolor and smoothed across voxels. Thy-1 is expressed in the cortex, DRD2 in the striatum (caudate/putamen). (A) Human brain, atlas section from Virtual Hospital: The Human Brain (<http://www.vh.org>). The voxel size was 3.3 mm. (B) Rat brain, coronal atlas section from Paxinos and Watson.<sup>24</sup> The voxel size was 1 mm. Coordinates in mm: IA, interaural; Br, bregma. (C) Mouse brain, coronal atlas section from the Mouse Brain Library (<http://www.mbl.org>).<sup>25</sup> The voxel size was 1 mm.

## Acknowledgments

Supported by the NIH/NIDA (DA015802, DA05010) NARSAD Young Investigator Award, Tobacco-Related Disease Research Program (11RT-0172), and Alzheimer's Association (IIRG-02-3609).

---

<sup>24</sup> G. Paxinos and C. Watson, "The Rat Brain in Stereotaxic Coordinates." Academic Press, Orlando, FL, 1986.

<sup>25</sup> R. W. Williams, *Results Probl. Cell Differ.* **30**, 21 (2000).

# [16] MR-Intracranial Compliance and Pressure: A Method for Noninvasive Measurement of Important Neurophysiologic Parameters

By NOAM ALPERIN

## Introduction

Advances in magnetic resonance imaging (MRI) technology over the last decade resulted with dramatic decrease in MR image acquisition time from minutes to few milliseconds. With short acquisition time it is now possible to capture dynamic biologic processes such as the beating of the heart or changes in cerebral blood oxygenation level following neural activation. The strictly anatomic information provided by MRI early on is now augmented with functional information. MRI, being a noninvasive imaging modality, therefore offers new capabilities for visualization and quantitation of biologic processes in humans.

A recently developed methodology to study cerebral physiology through dynamic measurements of blood and cerebrospinal fluid (CSF) flow is described in this chapter. The MRI-based method provides measurements of the following physiologic parameters: total cerebral blood flow (TCBF), intracranial compliance (the inverse of elastance), and intracranial pressure (ICP). In addition to the overall compliance of the intracranial compartment, the method provides information on the biomechanical state of sub-compartments of the intracranial space such as the cerebral vasculature (e.g., the cerebral vascular compliance). These physiologic parameters are important for characterization of the hemodynamic and hydrodynamic state of the craniospinal system (i.e., the craniospinal biomechanical state). The biomechanical state of the craniospinal system is not constant; it changes with normal activities (e.g., change in body posture), due to aging and by head trauma and diseases (e.g., intracranial tumors, hydrocephalous,